Hindawi
Complexity
Volume 2022, Article ID 5446369, 11 pages
https://doi.org/10.1155/2022/5446369

Research Article

Dynamics Analysis and Intermittent Energy Feedback Control of m-HR Neuron Model under Electromagnetic Induction

Jiankui Peng[1,2] **and Suoping Li**[1,3]

[1]*School of Electrical and Information Engineering, Lanzhou University of Technology, Lanzhou 730050, China*
[2]*School of Education, Lanzhou University of Arts and Science, Lanzhou 730010, China*
[3]*School of Sciences, Lanzhou University of Technology, Lanzhou 730050, China*

Correspondence should be addressed to Suoping Li; lsuop@163.com

Received 31 May 2022; Revised 25 July 2022; Accepted 27 August 2022; Published 23 September 2022

Academic Editor: Karthikeyan Rajagopal

It is of great practical significance to fully reveal the global discharge characteristics of neurons in electromagnetic environment and design effective energy feedback strategy for accurate prediction of neural information. Considering the effect of electromagnetic induction, a four-dimensional modified Hindmarsh–Rose (m-HR) neuron model is established, and its discharge mechanism is revealed by analyzing the existence and stability of equilibrium point of the model. Extensive numerical results confirm that the model has classical period-doubling bifurcation, period-adding bifurcation, and comb-shaped chaotic structure. Importantly, a new intermittent energy feedback controller is designed by improving the traditional energy feedback control strategy, which can effectively modulate the desired discharge modes under the cost-optimal energy consumption. Meanwhile, it should be emphasized that the intermittent control scheme has a wider range of regulation and robustness, which can be applied to other dynamical systems to obtain the desired oscillation modes. This will improve the beneficial discussion for the construction of brain-like intelligent network and efficient regulation.

1. Introduction

Complex neuron firing activities and dynamic phenomena are involved in neural information processing, including resting state and periodic and chaotic discharge modes [1–3]. Considering the complex electrophysiological activities, the most important factor regulating the discharge activities of nerves is the adaptive adjustment of external stimuli and electromagnetic induction [4]. Accordingly, a large number of studies have reported on the dynamic behavior of neurons and their networks under electromagnetic induction feedback [5–8]. In general, positive feedback induced current or electromagnetic radiation helps to stimulate neurons to produce multiple patterns of electrical activity [9]. Importantly, Wu and Gu [10] found that the built-in parameters of the memristor were decisive factors in regulating the neuron discharge activity. By appropriately selecting the parameter values of the memristor, the positive feedback memory current inhibited the neuron cluster discharge activity, while the inhibitory memory current promoted the neuron electrical activity [11]. Qiao and An [12] confirmed that magnetic field can induce the HR neuron model to produce bistable phenomenon, hidden discharge mode, and even mixed mode oscillation and further proposed strategies to control hidden discharge activities. Meanwhile, electric field can also stimulate the hidden dynamic behavior and multiattractor coexistence of neurons [13]. Lin et al. [14] found that the Hopfield neural network has the coexistence phenomenon of hidden extremely stability and hyperchaotic attractor under electromagnetic radiation. Moreover, the type of memristor is also a key factor leading to multistability of neurons. Bao et al. [15] realized the feedback mechanism of induced current on the membrane potential of Morris–Lecar (ML) neuron by introducing hyperbolic tangent memristor. The study found that the model not only had classical period-doubling

bifurcation and period-adding bifurcation with chaos bifurcation cascade but also revealed its initial value sensitivity by simulating the fractal structure of the attraction domain. Li et al. [16] used numerical methods to reveal that discrete Rulkov neurons with electromagnetic induction feedback have periodic discharge, transient chaos, and even hyperchaotic discharge modes, which mainly depend on the built-in parameters of the memristor. Peculiarly, Parastesh et al. [17] explored the hyperchaotic behaviors of the HR neuron model by introducing the discontinuous electromagnetic induction effect. Wang et al. [18] explored the complex chaotic behavior and multistability of an HR neuron with electromagnetic flux and external excitation. Rajagopal et al. [19] explored the generation mechanism and control method of spiral waves in an ML neuron network with electromagnetic induction. Karthikeyan et al. [20] analyzed the effect of induced current on bifurcation patterns and spatiotemporal responses of the coupling network of a temperature-sensitive ML neuron. It is worth mentioning that memristors have important applications in stimulating multistability of continuous and non-smooth systems [21–23]. Besides, magnetic flux coupling plays a constructive role in realizing network synchronization and excitation of spiral waves [24, 25]. These results enrich the dynamic phenomena of neurons in complex electromagnetic environment and provide useful discussion for related physiological experiments. However, how to predict the electrical activity and global evolution of neurons through local dynamic analysis is a field worthy of further exploration, which is also one of the problems to be discussed in this paper.

Generally, the oscillation of the system depends on the continuous supply and release of energy, and accordingly, the state stability of the system can be helped by appropriately adjusting the feedback of energy [26]. Song et al. [27] found that the energy storage of neurons depends on external stimuli and electrical patterns, and periodic or chaotic discharge states contribute to the rapid release of energy. Yang et al. [28] showed that high-frequency electromagnetic radiation has a smaller impact on nervous system than low-frequency electromagnetic radiation, while low-frequency electromagnetic radiation with large amplitude is conducive to energy injection and induced discharge mode transformation. Guo et al. [29] proposed the energy feedback control chaos strategy and confirmed that proper energy regulation can effectively suppress chaos and make it reach the desired periodic oscillation state. Wu et al. [30] designed an energy feedback method to properly control the hidden attractor and verified the effectiveness of the modified scheme based on extensive numerical simulations. What is noteworthy is that An and Qiao [31] disclosed the bistable features, global bifurcation structure, and mixed mode oscillation of HR neurons under electromagnetic induction, and a new energy feedback method was proposed to eliminate hidden discharge activities.

In conclusion, the above discussion verifies the internal constraint relationship between energy and oscillation mode of the system. Nevertheless, how to improve the efficiency of energy feedback control? It is worthy of further investigation to achieve the regulation of system oscillation state under the small energy loss, and this is another issue that deserves our attention.

The organization of this paper is as follows. In Section 2, considering the electromagnetic induction effect, the m-HR neuron model under the action of magnetic field is established. In Section 3, the existence and stability conditions of the equilibrium point of the model are determined, and the relationship between the stability region of the equilibrium point and the discharge mode is analyzed. Meanwhile, the global dynamics characteristics of the model are revealed based on the two-parameter bifurcation diagram and its maximum Lyapunov exponential diagram. In Section 4, the intermittent energy feedback strategy is proposed, and the high efficiency of the method is verified. Finally, the relevant research conclusions are summarized.

2. Model Description

Tsaneva et al. [32] constructed the m-HR neuron model on the basis of the classical HR neuron model [33] and provided it with more abundant discharge modes and global bifurcation laws while maintaining a simple mathematical structure [34]. Considering that neural information involves complex electromagnetic environment in the process of processing, this paper realizes the feedback modulation of flux variable on membrane potential by introducing magneto-memristor, and its dynamic system expression is

$$\begin{cases} \dot{x} = -s\left(-ax^3 + x^2\right) - y - bz + I + I_e, \\ \dot{y} = \varepsilon\left(x^2 - y\right), \\ \dot{z} = u\left(sa_1 x + b_1 - kz\right), \\ \dot{\phi} = k_1 x - k_2 \phi, \end{cases} \tag{1}$$

where x, y, z, and ϕ represent membrane potential, potassium ion current fast variable, calcium ion current slow variable, and flux variable, respectively. The feedback memory current of electromagnetic field to membrane voltage is I_e; in order to realize the coupling of flux variable and membrane potential, its mathematical expression is $I_e = -k_0(\alpha + 3\beta\phi^2)x$, where k_0 is the electromagnetic radiation intensity and α and β are the built-in parameters of the memristor. In addition, a, b, a_1, b_1, k, s, ε, and u are important parameters in regulating the electrical activity of neurons. During the numerical calculation, the reference values of parameters are selected from Ref. [32], which are expressed as $a = 0.5$, $b = 1$, $a_1 = -0.1$, $b_1 = -0.045$, $k = 0.2$, $s = -1.61$, $\varepsilon = 1$, $u = 0.01$, $I = 0$, $k_0 = 0.1$, $k_1 = 0.9$, $k_2 = 0.5$, $\alpha = 0.1$, and $\beta = 0.02$.

3. Stability of Equilibrium Point and Its Global Bifurcation Model

3.1. Stability Analysis. Actually, the firing mode of neurons is closely related to its equilibrium stability, that is, the stable equilibrium point has a resting state, while the unstable equilibrium point will stimulate the firing activity. Setting $\dot{x} = \dot{y} = \dot{z} = \dot{\phi} = 0$, then it can be inferred that

$$\begin{cases} -s\left(-ax^3 + x^2\right) - y - bz + I + I_e = 0, \\ x^2 - y = 0, \\ sa_1 x + b_1 - kz = 0, \\ k_1 x - k_2 \phi = 0. \end{cases} \tag{2}$$

According to (2), the zero-point equation is

$$F(x) = Q_0 x^3 + Q_1 x^2 + Q_2 x + Q_3 = 0, \tag{3}$$

where

$$\begin{cases} Q_0 = \left(as - 3\beta k_0 k_1^2 / k_2^2\right), \\ Q_1 = -(s+1), \\ Q_2 = -\left(a_1 bs/k + k_0 \alpha\right), \\ Q_3 = -bb_1/k + I. \end{cases} \tag{4}$$

If $F(x_e) = 0$, the equilibrium point of system (1) is $P_e = (x_e, x_e^2, (sa_1 x_e + b_1)/k, k_1 x_e/k_2)$.

Let $F_1 = Q_1^2 - 3Q_0 Q_2$, $F_2 = Q_1 Q_2 - 9Q_0 Q_3$, and $F_3 = Q_2^2 - 3Q_1 Q_3$, so the total discriminant is $\Delta = F_2^2 - 4F_1 F_3$ and the equilibrium point of system (1) exists in the following three cases.

When $\Delta > 0$, system (1) has only one equilibrium point, which is expressed as

$$\begin{cases} x_e = \left(-Q_1 - \left(\sqrt[3]{X_1} + \sqrt[3]{X_2}\right)\right), \\ y_e = x_e^2, \\ z_e = \left(a_1 s x_e + b_1\right)/k, \\ \phi_e = k_1 x_e / k_2, \end{cases} \tag{5}$$

where $X_{1,2} = A_1 Q1 + 3Q_0 \left(-F_2 \pm \sqrt{F_2^2 - 4F_1 F_3}\right)/2$.

When $\Delta = 0$, system (1) has two equilibrium points, which are expressed as

$$\begin{cases} x_{e_1} = -Q_1/Q_0 + Y, x_{e_2} = -Y/2_0, \\ y_{e_i} = x_{e_i}^2, \\ z_{e_i} = \left(a_1 s x_{e_i} + b_1\right)/k, \\ \phi_{e_i} = k_1 x_{e_i}/k_2, \end{cases} \tag{6}$$

where $i = 1, 2$, $Y = F_2/F_1$ $(F_1 \neq 0)$.

When $\Delta < 0$, system (1) has three equilibrium points, which are expressed as

$$\begin{cases} x_{e_i} = \left(-Q_1 - 2\sqrt{F_1}\cos\left((2\pi i + \theta)/3\right)\right)/3F_0, \\ y_{e_i} = x_{e_i}^2, \\ z_{e_i} = \left(a_1 s x_{e_i} + b_1\right)/k, \\ \phi_{e_i} = k_1 x_{e_i}/k_2, \end{cases} \tag{7}$$

where $i = 1, 2, 3$, $\theta = \arccos T$, $T = (2F_1 Q_1 - 3Q_0 F_2)/2\sqrt{F_1^3}$, $F_1 > 0, -1 < T < 1$.

The stability of system (1) at equilibrium point $P_e = (x_e, y_e, z_e, \phi_e)$ is determined by the Jacobian matrix J, which is expressed as

$$J = \begin{bmatrix} 3asx_e^2 - 2sx_e - k_0(\alpha + 3\beta\phi_e) & -1 & -b & -6k_0\beta x_e \phi_e \\ 2x_e & -1 & 0 & 0 \\ a_1 su & 0 & -ku & 0 \\ k_1 & 0 & 0 & -k_2 \end{bmatrix}. \tag{8}$$

In order to facilitate the analysis of the stability of equilibrium point and bifurcation behavior of system (1), I and k_0 are selected as bifurcation parameters, and the other parameters are taken as reference values. Based on Matcont software [35], stability distribution of the equilibrium point of system (1) can be quickly obtained, as visible in Figure 1(a), where I-1, I-2, and I-3 regions represent the stable nodes, stable focal point, and the unstable focal point, respectively. Further, the Hopf bifurcation is identified by red curve. It can be seen that complex equilibrium stability regions are distributed on the parameter plane, in which the I-2 region is transformed into the I-3 region through Hopf bifurcation behavior. Interestingly, Figure 1(b) reveals that the unstable equilibrium can excite various discharge modes in the I-3 and 4 regions, in which different colors represent different discharge states, and different discharge modes are distinguished by corresponding numerical values. For example, the number 0 represents the quiescent state, the numbernn denotes the period-n ($n = 1, 2, \cdots, 19$) discharge state, and the white area indicates the higher periodic discharge activities or chaos. It can be seen that Figures 1(a) and 1(b) have good complementarity, and together they reveal the built-in mechanism of the neuron to produce complex discharge activities.

3.2. Two-Parameter Bifurcation Analysis. Surely, in the complex physiological environment, there are many factors that affect the firing activity of neurons and lead to the change of the benchmark parameters of the system, while stimulating a variety of firing patterns. As a result, the study of electrical activity and bifurcation behavior in multiparameter space has important practical reference value. When $s \in [-1.70, -1.55]$, $b_1 \in [-0.060, -0.030]$, Figures 2(a) and 2(b) display the bifurcation diagram and the largest Lyapunov exponent, respectively, which confirms that the system has complex discharge mode and self-organization law. It can be seen that there is a large range of period-1 spiking region in the lower right part of the parameter plane, and with the gradual increase of parameters s and b_1, system (1) has a period-doubling bifurcation behavior and then eventually tends to comb-shaped chaotic region. Interestingly, a large number of tongue-shaped periodic regions exist in the upper right region of the parameter plane and are embedded in the comb chaotic region by means of period-doubling bifurcation and bifurcation segmentation.

To more intuitively reveal the self-organization rules of these tongue-shaped periodic regions, let $b_1 = -0.1789s - 0.3221$ and$s \in [-1.70, -1.55]$, that is, along the direction shown by the black line in Figure 2(a), with the gradual increase of

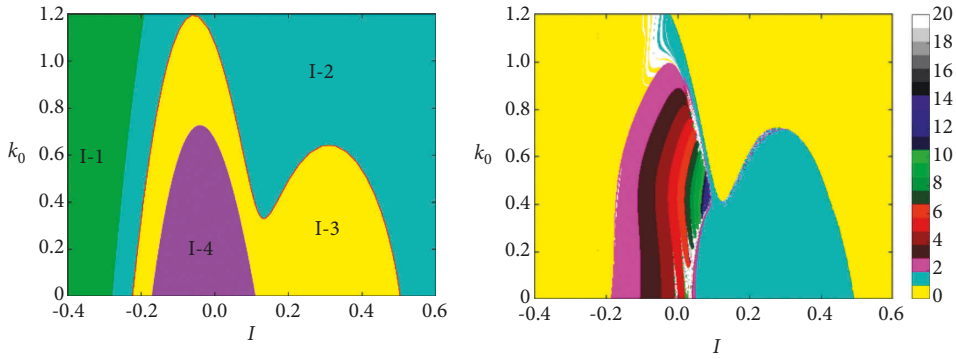

FIGURE 1: The local dynamics and global response of system (1) for $I \in [-0.4, 0.6]$, $k_0 \in [0, 1.2]$. (a) The stability distribution diagram. (b) Bifurcation diagram, where diverse discharge modes are identified by different color areas.

parameter s, the inter-spike interval (ISI) bifurcation diagram and the largest Lyapunov exponential diagram of system (1) are shown in Figures 3(a) and 3(b), respectively. The bifurcation sequence of the membrane potential x is as follows: period-2 bursting $\longrightarrow$ chaos via period-doubling bifurcation $\longrightarrow$ the chaotic state is transformed into periodic 3 bursting state by tangent bifurcation $\longrightarrow$ it leads to chaos again through period-doubling bifurcation $\longrightarrow \ldots \longrightarrow$ finally, the cluster discharge or chaotic state with higher period leads to the classical period-adding bifurcation with chaos mode [36]. This is also the internal reason why system (1) has the comb-shaped chaotic structure. Furthermore, the corresponding time of membrane potential x at points A, B, C, and D in Figure 2(a) is depicted in Figures 4(a)–4(d), respectively, so it can be known that system (1) is in period-3, period-5, period-7, and chaotic discharge state, respectively.

Similarly, in the parameter plane shown in Figures 2(c)–2(e), system (1) also has tongue-shaped periodic region and comb-shaped chaotic structure, in which its corresponding periodic region becomes narrower with the increase of the number of active periodic of bursting. Note that this bifurcation feature is common in all kinds of dynamical systems [37–39]. More precisely, Figure 2(c) manifests that the discharge mode mainly depends on parameter u for $I \in [0, 0.04]$, where the smaller the value of u is, the larger the corresponding period or chaos appears. Further, when $I \in [0.04, 0.05]$, parameter u has little effect on the bifurcation structure, whereas the inverse period-doubling bifurcation pattern occurs with the increase of parameter I. Figure 2(d) exhibits period-doubling bifurcation behavior with the increase of parameter $b_1 \in [-0.055, -0.053]$. Accordingly, when $b_1 \in [-0.053, -0.040]$, the period-adding bifurcation with chaos pattern is excited under the control of parameter u. Interestingly, as visible in Figure 2(e), parameter b also plays a decisive role in inducing the comb-shaped chaotic structure. In particular, for $s \in [-1.54, -1.46]$, $u \in [0.004, 0.022]$, system (1) as shown in Figure 2(f) only has periodic bursting pattern, and the transformation of various discharge modes is realized by period-adding bifurcation without chaos. More precisely, along the direction from top to bottom of the parameter plane, its bifurcation sequence is as follows: period-4 bursting $\longrightarrow$ period-5 bursting $\longrightarrow \ldots \longrightarrow$ finally it tends to higher periodic bursting activities. Moreover, when $I \in [0, 0.06]$, $k_1 \in [0, 1.0]$, system (1) only has a large range of periodic and chaotic discharge regions, as illustrated in Figure 2(g). The periodic regions on the left and right sides of the parameter plane lead to the chaotic region through period-doubling bifurcation. When $I \in [0, 0.06]$, $k_2 \in [0.2, 1.0]$, it can be seen from Figure 2(h) that system (1) only has a tongue-shaped period-5 bursting region embedded in the chaotic region. These numerical results fully reveal the global dynamic characteristics of system (1) and provide a useful discussion for the accurate prediction of neural discharge activity and evolution. It should be noted that Figures 3(a) and 3(b) illustrate the dynamics details of Figure 2(a). Since the quiescent state is transformed into various discharge modes through Hopf bifurcation behavior, which indicates that there is no Hopf bifurcation behavior in Figure 2(a) (i.e., there is no quiescent state region).

4. Intermittent Feedback Control Based on Hamiltonian Energy

The different firing modes of neurons are closely related to the energy flow, and the continuous supply and release of energy is the key to maintain the system oscillation. For any autonomous dynamical system $\dot{X} = f(X)$, $f(X)$ can be decomposed into $f(X) = f_c(X) + f_d(X)$ based on Helmholtz theory [20], where $f_c(X)$ represents the vortex field, which has no effect on the direction of the phase trajectory of the system movement, and its relationship with the Hamiltonian energy H satisfies $\nabla H^T f_c(X) = 0$. However, $f_d(X)$ indicates the gradient field, which can constrain the phase trajectory of system operation and satisfy $\dot{H} = \nabla H^T f_d(X)$. Thus, system (1) can be expressed as follows:

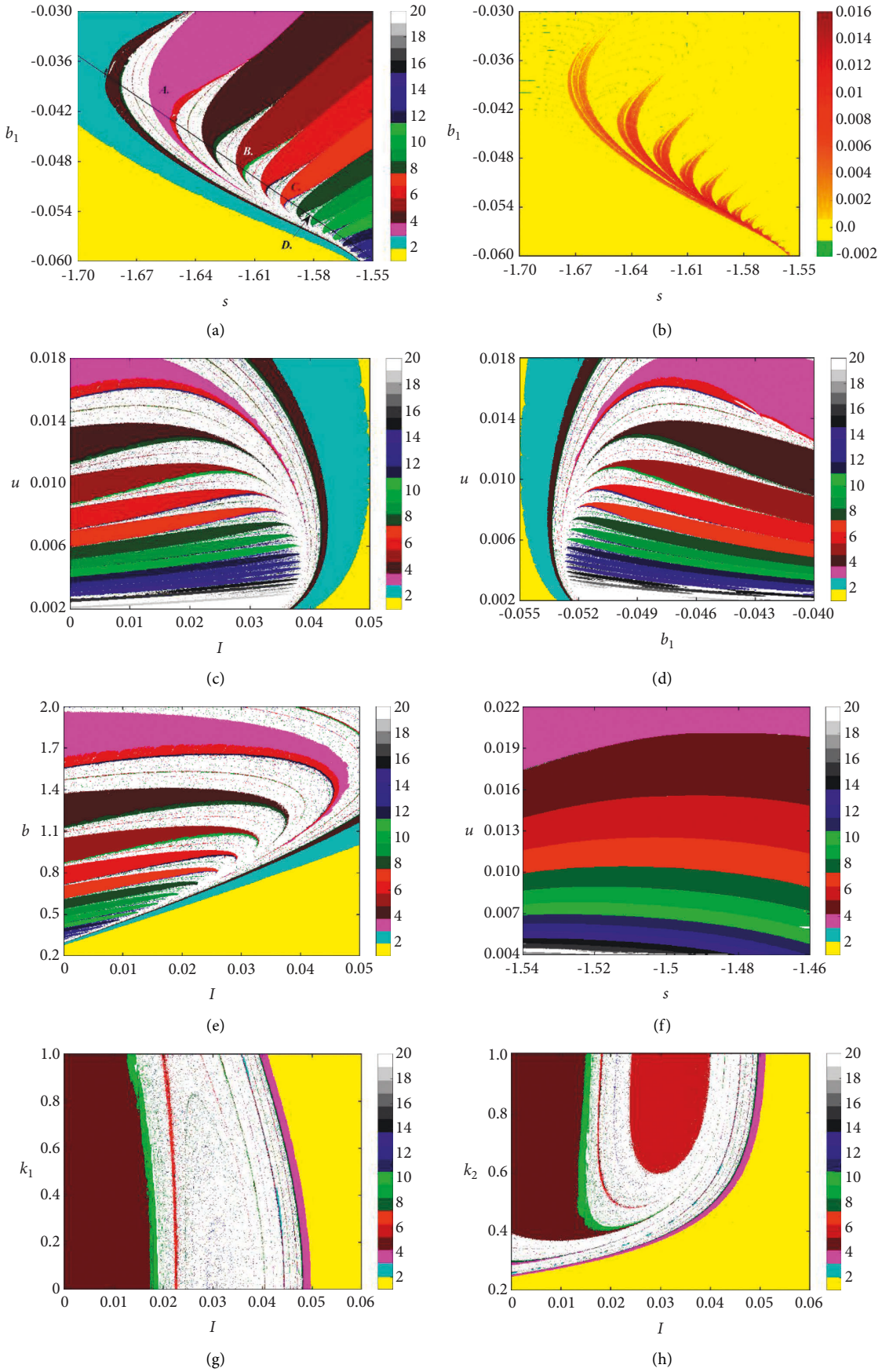

FIGURE 2: Dynamic details of system (1) for different parameter combinations: (a) $s \in [-1.70, -1.55]$, $b_1 \in [-0.06, -0.03]$; (b) the largest exponent of (a); (c) $I \in [0, 0.05]$, $u \in [0.002, 0.018]$; (d) $b_1 \in [-0.055, -0.040]$, $u \in [0.002, 0.018]$; (e) $I \in [0, 0.05]$, $b \in [0.2, 2]$; (f) $s \in [-1.54, -1.46]$, $u \in [0.004, 0.022]$; (g) $I \in [0, 0.06]$, $k_1 \in [0, 1.0]$; (h) $I \in [0, 0.06]$, $k_2 \in [0.2, 1.0]$.

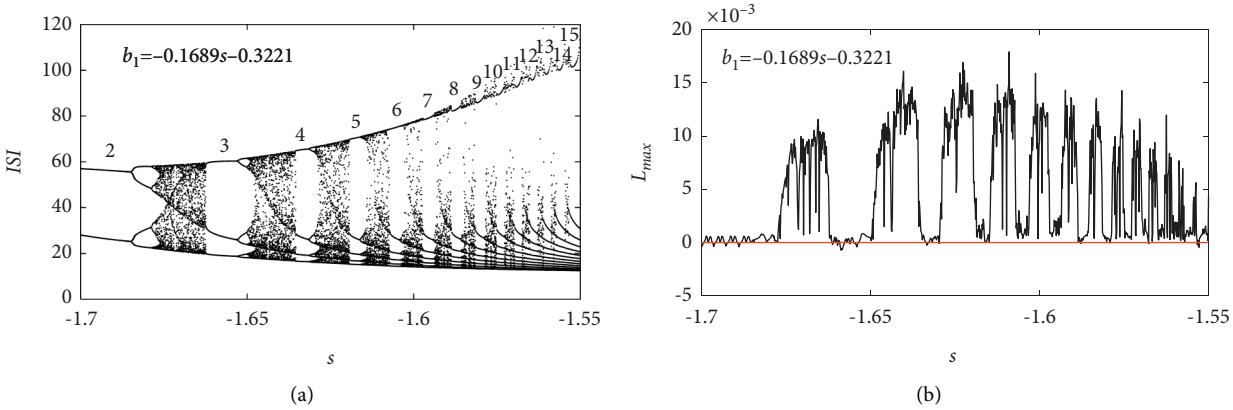

FIGURE 3: Bifurcation diagram (a) and the largest Lyapunov exponent diagram (b) along the black line ($b_1 = -0.1689s - 0.3221$, $s \in [-1.7, -1.55]$) in Figure 1(a).

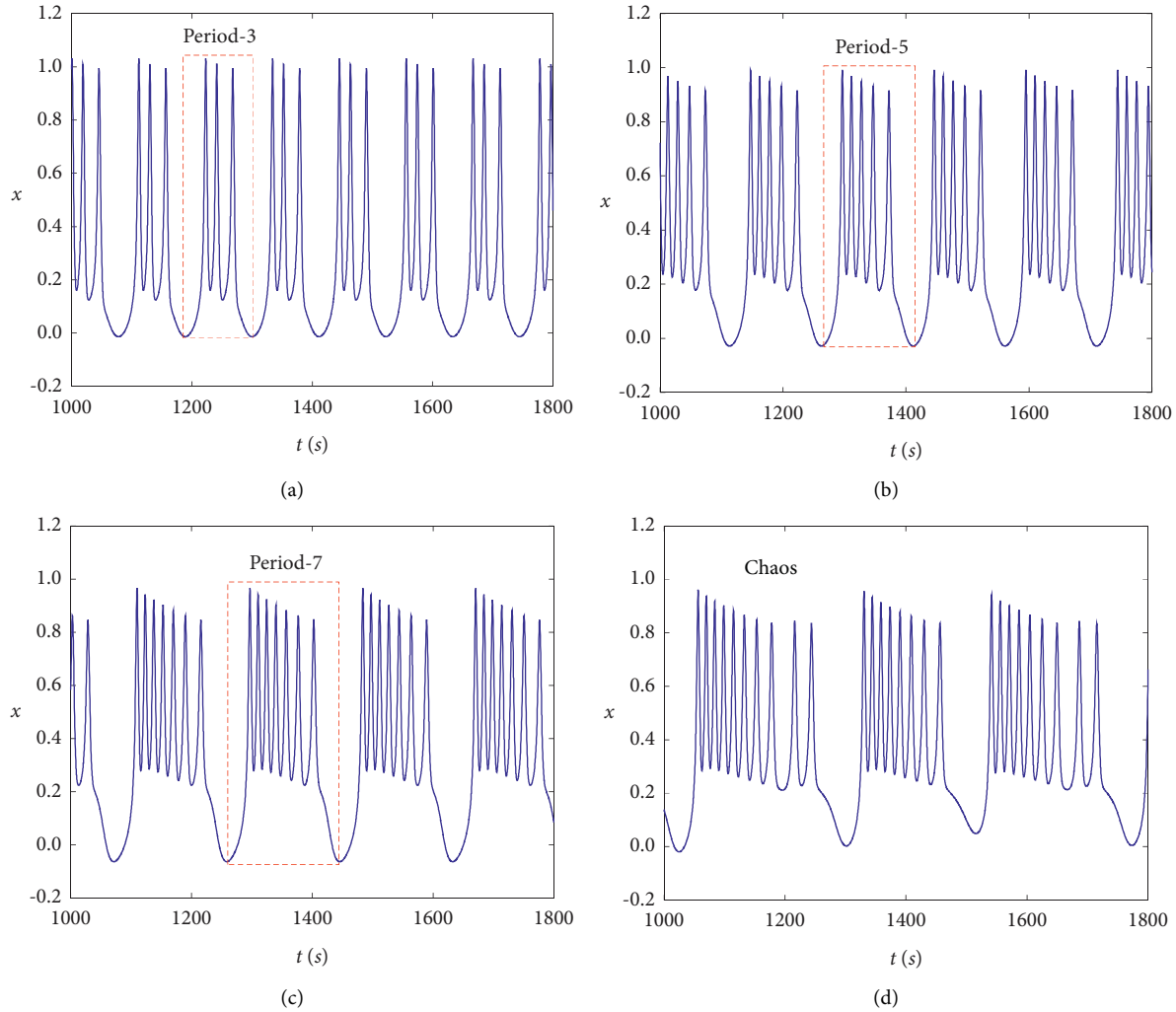

FIGURE 4: The time response diagrams for different parameters s and b_1: (a) $(s, b_1) = (-1.655, -0.039)$, (b) $(s, b_1) = (-1.614, -0.047)$, (c) $(s, b_1) = (-1.588, -0.051)$, and (d) $(s, b_1) = (-1.585, -0.055)$.

$$\begin{bmatrix}\dot{x}\\ \dot{y}\\ \dot{z}\\ \dot{\phi}\end{bmatrix} = \dot{X} = f(X) = \begin{bmatrix}-y-bz-\phi\\ \varphi x^2\\ u(sa_1x+b_1)\\ k_1x\end{bmatrix} + \begin{bmatrix}-s\left(-ax^3+x^2\right)+I+I_e+\phi\\ -\varphi y\\ -ukz\\ -k_2\phi\end{bmatrix} = f_c(X)+f_d(X). \tag{9}$$

It can be obtained from $\nabla H^T f_c(x) = 0$ that

$$(-y-bz-\phi)\frac{\partial H}{\partial x}+\varphi x^2\frac{\partial H}{\partial y}+u(sa_1x+b_1)\frac{\partial H}{\partial z}+k_1x\frac{\partial H}{\partial \phi}=0. \tag{10}$$

The following equation can be obtained from (8):

$$\begin{aligned}(-y-bz-\phi)\frac{\partial H}{\partial x} &= \varphi x^2\frac{\partial H}{\partial y},\\ (-y-bz-\phi)\frac{\partial H}{\partial x} &= u(sa_1x+b_1)\frac{\partial H}{\partial z},\\ (-y-bz-\phi)\frac{\partial H}{\partial x} &= k_1x\frac{\partial H}{\partial \phi},\end{aligned} \tag{11}$$

and then one can get

$$\begin{aligned}\frac{1}{3}\varphi x^3+\frac{1}{2}(-y-bz-\phi)^2 &= 0,\\ \frac{ub}{2sa_1}(sa_1x+b_1)^2+\frac{1}{2}(-y-bz-\phi)^2 &= 0,\\ \frac{1}{2}k_1x^2+\frac{1}{2}(-y-bz-\phi)^2 &= 0.\end{aligned} \tag{12}$$

The preliminary result can be obtained as follows:

$$\begin{aligned}H(x,y,z) = \frac{1}{3}\varphi x^3+\frac{bu}{2sa_1}(sa_1x+b_1)^2\\ +\frac{1}{2}(y+bz+\varphi)^2+\frac{1}{2}k_1x^2.\end{aligned} \tag{13}$$

To ensure the uniqueness of Hamiltonian energy, it is important and necessary to verify the relation $\dot{H} = \nabla H^T f_d(x)$. Thus, the derivative of Hamiltonian energy H can be obtained:

$$\begin{aligned}\dot{H}(x,y,z) &= \left(\varphi x^2+bu(sa_1x+b_1)+k_1x\right)\dot{x}+(y+bz+\phi)\dot{y}+b(y+bz+\phi)\dot{z}+(y+bz+\phi)\dot{\phi}\\ &= \left(\varphi x^2+bu(sa_1x+b_1)+k_1x\right)\left(-s\left(-ax^3+x^2\right)-y-bz+I+I_e+\phi-\phi\right)+(y+bz+\phi)\left(\varphi\left(x^2-y\right)\right)\\ &\quad +b(y+bz+\phi)\left(u(sa_1x+b_1-kz)\right)+(y+bz+\phi)\left(k_1x-k_2\phi\right)\\ &= \varphi x^2(-y-bz-\phi)+bu(sa_1x+b_1)(-y-bz-\phi)+k_1x(-y-bz-\phi)\\ &\quad +\left(\varphi x^2+bu(sa_1x+b_1)+k_1x\right)\left(-s\left(-ax^3+x^2\right)+I+I_e+\phi\right)+(y+bz+\phi)\varphi x^2\\ &\quad +(y+bz+\phi)(-\varphi y)+b(y+bz+\phi)\left(u(sa_1x+b_1)\right)+b(y+bz+\phi)(-ukz)\\ &\quad +(y+bz+\phi)k_1x+(y+bz+\phi)\left(-k_2\phi\right)\\ &= \left(\varphi x^2+bu(sa_1x+b_1)+k_1x\right)\left(-s\left(-ax^3+x^2\right)+I+I_e+\phi\right)+(y+bz+\phi)(-\varphi y)\\ &\quad +b(y+bz+\phi)(-ukz)+(y+bz+\phi)\left(-k_2\phi\right)\\ &= \nabla H^T f_d(X).\end{aligned} \tag{14}$$

In order to reduce the energy loss in the control process and improve the control effect of Hamiltonian energy, it is necessary to improve the traditional energy feedback controller. Two types of energy feedback control model are applied to system (1) based on energy (9) as follows:

$$\begin{cases}\dot{x} = -s\left(-ax^3+x^2\right)-y-bz+I+I_e(\phi)-\Gamma_i(H),\\ \dot{y} = \varphi\left(x^2-y\right),\\ \dot{z} = u(sa_1x+b_1-kz),\\ \dot{\phi} = k_1x-k_2\phi,\\ \dot{H} = \nabla H^T f_d(x)-nH,\end{cases} \tag{15}$$

where $\Gamma_i(H)$, $(i=1,2)$, denote the traditional Hamiltonian energy feedback controller and intermittent feedback controller, where their expressions are defined as $\Gamma_1(H) = mHx$, $\Gamma_2(H) = m(\theta(H-H_{\min})+\theta(H_{\max}-H))x$, respectively. $\theta(\chi)$ represents the Heaviside function, in which $\theta(\chi)=0$ for $\chi\le 0$ and $\theta(\chi)=1$ for $\chi>0$. It can be seen that only when $H\in[H_{\min},H_{\max}]$, the controller $\Gamma_2(H)$ can operate intermittently, which reduces energy consumption and improves energy utilization efficiency at the same time. Furthermore, m represents the feedback gain of Hamiltonian energy on the membrane potential x. n is the adaptive adjustment intensity of the energy controller, which is the key to ensure the stability of the controller. Importantly, the periodic mode or chaotic discharge activities of system (1)

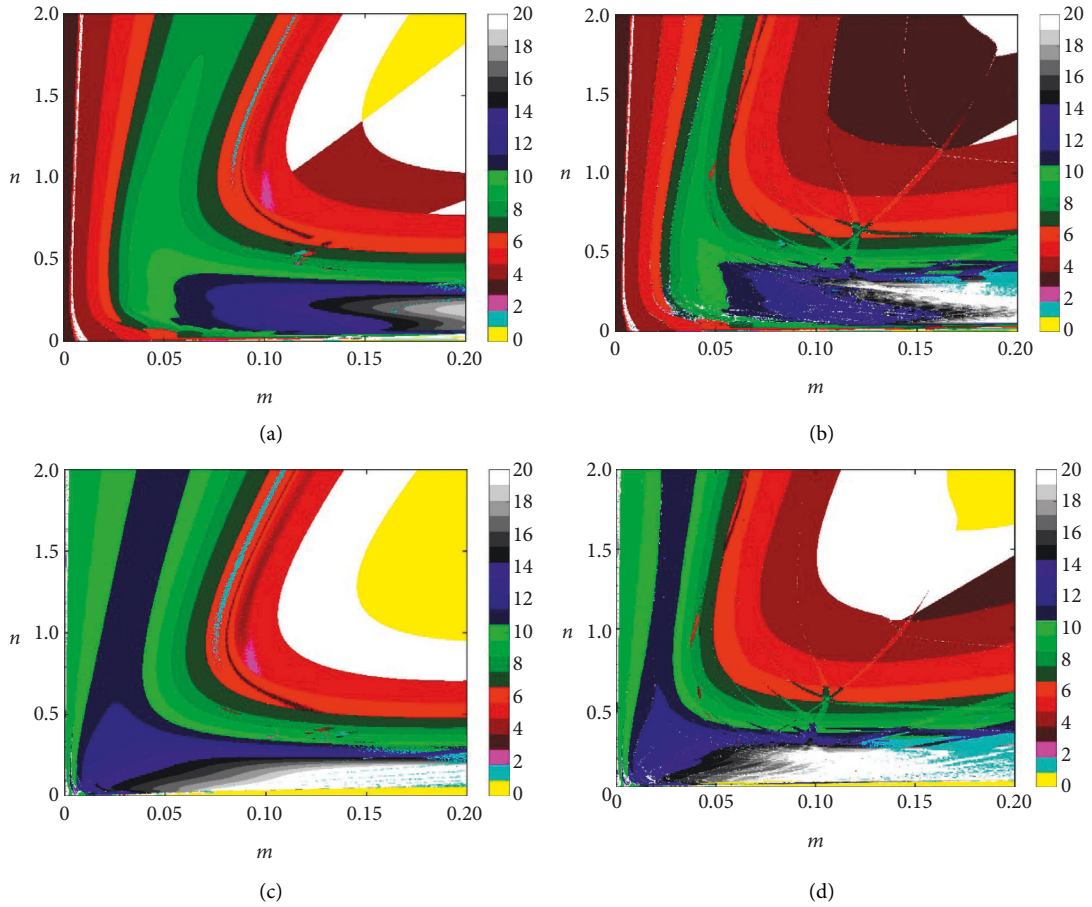

FIGURE 5: Discharge mode evolution diagram of system (10) under different controllers Γ_i, $(i = 1, 2)$. When $(s, b_1) = (-1.655, -0.039)$, (a) evolution diagram under Γ_1; (b) evolution diagram under Γ_2. When $(s, b_1) = (-1.585, -0.055)$, (c) evolution diagram under Γ_1; (d) evolution diagram under Γ_2.

can be effectively regulated by adjusting parameters m and n. Meanwhile, the neuron absorbs or releases energy to achieve the evolution of the neuron firing patterns.

It is important to control the periodic oscillations of neurons effectively to maintain the effective transmission, reception, and response of physiological information in the nervous system. When $(s, b_1) = (-1.655, -0.039)$, system (1) is in period-3 bursting state, and its corresponding time response is shown in Figure 4(a). Accordingly, it is necessary to explore the control effect of the traditional controller $\Gamma_1(H)$. When $m \in [0, 0.20]$, $n \in [0, 2.0]$, the results in Figure 5(a) confirmed that system (10) can produce a wide range of quiescent state, bursting activities with a period of 4–19, and even chaotic state, which implies that controller $\Gamma_1(H)$ can effectively adjust the discharge modes of system (1) by applying appropriate feedback stimulus. Importantly, to improve its control efficiency and reduce energy loss, let $H_{\min} = -0.1$ and $H_{\max} = 0.1$, and the control effect of controller $\Gamma_2(H)$ on system (1) is illustrated in Figure 5(b). Compared with Figure 5(a), its periodic oscillation region is significantly larger, in which the control parameters can be adjusted more widely. Accordingly, the region of its quiescent state and chaotic oscillation is small, which indicates that the control effect of controller $\Gamma_2(H)$ on periodic oscillation is obviously beneficial to controller $\Gamma_1(H)$, and its control process consumes less energy. To display the control effect of controller $\Gamma_2(H)$, for convenience, $n = 0.2$ is selected. Figures 6(a)–6(d) manifest the time responses of the membrane voltage and Hamiltonian energy of system (10) under different feedback gains, when parameter m is fixed to 0.04, 0.08, 0.12, and 0.16, respectively. It is observed that the energy depends critically on the parameters of the system and the corresponding electrical activities. Meanwhile, since each firing pulse is an energy-consuming process, the energy decreases, while the energy in the corresponding quiescent state increases. Moreover, it should be emphasized that the periods of these electrical activities are consistent with their Hamilton energy, indicating that it is feasible to determine the discharge modes of neuronal systems by analyzing the energy. These results indicate that higher periodic bursting can be excited by increasing the strength of feedback gain m.

The chaotic oscillations of neurons have an important effect on the cognition, memory, and physiological activities of various organisms. Consequently, it is of great application value to achieve the desired stable discharge states by controlling the chaotic discharge mode of neurons. For

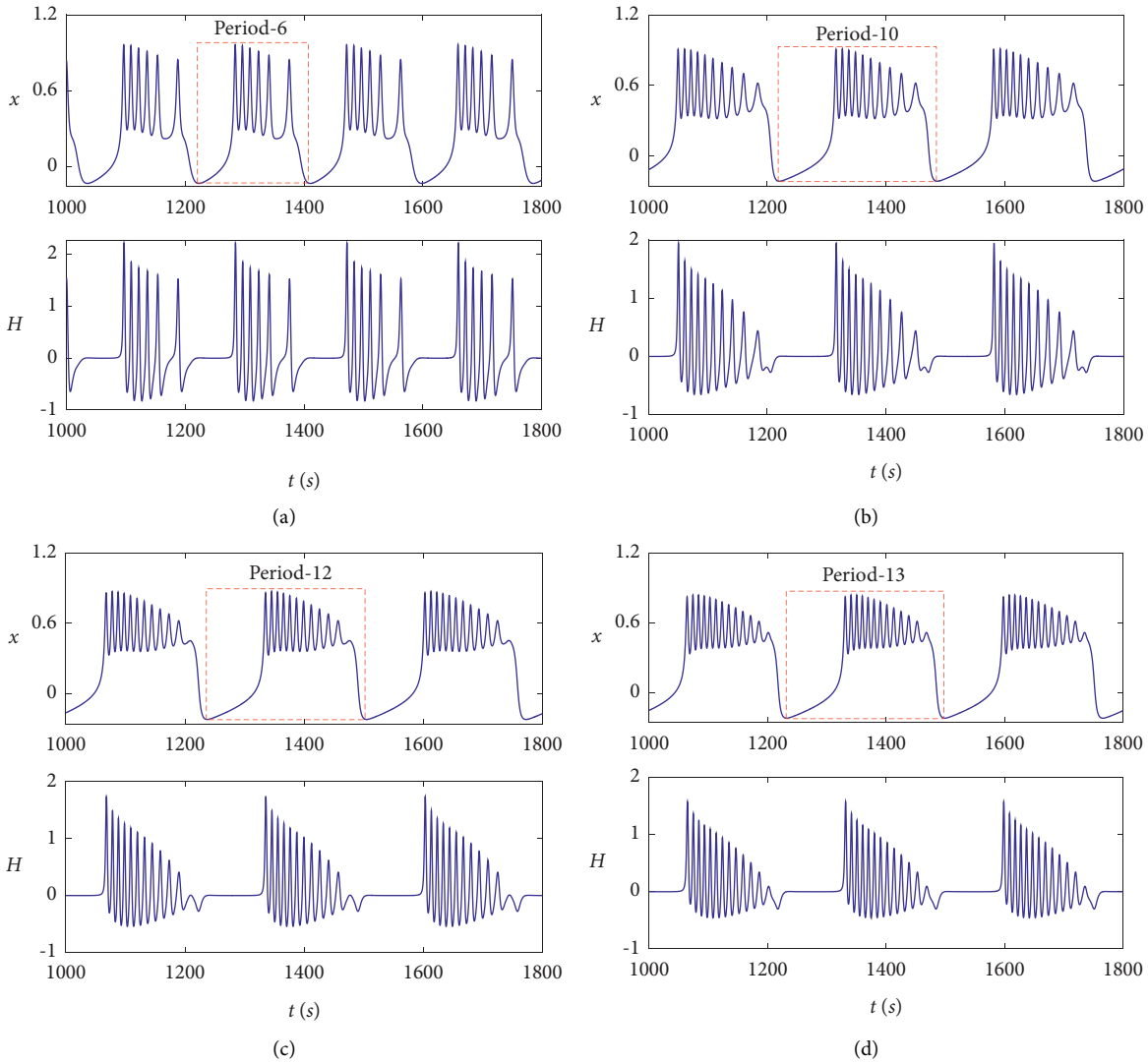

FIGURE 6: When $n = 0.2$, the discharge mode of system (10) and the responses of Hamiltonian energy under the feedback adjustment of controller $\Gamma_2(H)$: (a)$m = 0.04$; (b)$m = 0.08$; (c)$m = 0.12$; (d)$m = 0.16$.

$(s, b_1) = (-1.585, -0.055)$, system (1) is in chaotic bursting state, and its corresponding time response is exhibited in Figure 4(d). Similarly, Figures 5(c) and 5(d) show the discharge evolution diagrams under the control of controllers $\Gamma_1(H)$ and $\Gamma_2(H)$, respectively. Although the two controllers can effectively control chaotic discharge states and make them excite various discharge modes, the range of cycle region in Figure 5(d) is obviously larger, indicating that the control effect of controller $\Gamma_2(H)$ is obviously better than that of controller $\Gamma_1(H)$. Meanwhile, the energy consumption of the controller can be limited in the process of regulating the firing activity of neurons. In Ref. [12], the subcritical Hopf bifurcation stability of the e-HR neuron model was controlled by the washout filter to eliminate bistability (or hidden electrical activities). In this paper, however, the desired discharge modes are controlled by designing Hamilton intermittent feedback scheme. As a result, it can be seen that the control methods and objectives in this paper are completely different from those in Ref. [12].

5. Conclusion

In this paper, the local stability and global bifurcation features of the m-HR neuron model under electromagnetic induction are studied, and an efficient Hamiltonian energy feedback controller is improved to achieve the desired electrical activities. Firstly, the equilibrium stability and Hopf bifurcation behavior of the system are explored based on Matcont software, which is of great application to accurately predicting the firing modes of neurons. Further, the internal relationship between the equilibrium stability and the discharge pattern is disclosed, in which the stable equilibrium induced a quiescent state. Correspondingly, the stable equilibrium point becomes unstable by Hopf bifurcation, resulting in various discharge modes being excited (see Figure 1(b)). Secondly, it is confirmed that system (1) has the classical comb-shaped chaotic structure and period-adding bifurcation mode in the multiparameter spaces via multiple numerical tools, including the two-parameter

bifurcation and the largest Lyapunov exponential diagrams. Finally, the traditional Hamiltonian energy controller is improved, in which the controller can not only effectively adjust the periodic bursting, leading to producing higher periodic bursting modes, but also suppress chaotic discharge behavior and make it produce a wide range of periodic oscillation mode under the intermittent feedback. Importantly, this provides far better feedback than traditional persistence controllers, with a wider range of adjustable parameters and less energy loss. Moreover, we will further investigate the synchronization of coupled systems or networks with mismatched parameters by intermittent energy feedback.

Data Availability

The data that supports the findings of this study are available in this article.

Conflicts of Interest

The authors declare that they have no conflicts of interest.

Acknowledgments

This study was supported by the Fund of Department of Education of Gansu Province under grant no. 2022 A-172, the Hongliu First Discipline Development Project of Lanzhou University of Technology under grant no. 25-225305, and the National Natural Science Foundation of China under grant no. 61663024.

References

[1] S. K. Maran, F. H. Sieling, and K. Demla, "Responses of a bursting pacemaker to excitation reveal spatial segregation between bursting and spiking mechanisms," *Journal of Computational Neuroscience*, vol. 31, no. 2, pp. 419–440, 2011.

[2] E. M. Izhikevich, "Neural excitability, spiking and bursting," *International Journal of Bifurcation and Chaos in Applied Sciences and Engineering*, vol. 10, no. 6, pp. 1171–1266, 2000.

[3] A. Mondal, A. Mondal, S. Kumar Sharma, R. Kumar Upadhyay, and C. G. Antonopoulos, "Spatiotemporal characteristics in systems of diffusively coupled excitable slow-fast FitzHugh-Rinzel dynamical neurons," *Chaos: An Interdisciplinary Journal of Nonlinear Science*, vol. 31, no. 10, p. 103122, 2021.

[4] J. Ma and J. Tang, "A review for dynamics of collective behaviors of network of neurons," *Science China Technological Sciences*, vol. 58, no. 12, pp. 2038–2045, 2015.

[5] M. Lv, C. N. Wang, G. D. Ren, J. Ma, and X Song, "Model of electrical activity in a neuron under magnetic flow effect," *Nonlinear Dynamics*, vol. 85, no. 3, pp. 1479–1490, 2016.

[6] F. Q. Wu, C. N. Wang, W. Y. Jin, and J. Ma, "Dynamical responses in a new neuron model subjected to electromagnetic induction and phase noise," *Physica A: Statistical Mechanics and Its Applications*, vol. 469, pp. 81–88, 2017.

[7] H. Bao, A. H. Hu, W. B. Liu, and B. Bao, "Hidden bursting firings and bifurcation mechanisms in memristive neuron model with threshold electromagnetic induction," *IEEE Transactions on Neural Networks and Learning Systems*, vol. 31, no. 2, pp. 502–511, 2020.

[8] H. R. Lin, C. H. Wang, Q. L. Deng, C. Xu, Z. Deng, and C. Zhou, "Review on chaotic dynamics of memristive neuron and neural network," *Nonlinear Dynamics*, vol. 106, no. 1, pp. 959–973, 2021.

[9] M. Lv and J. Ma, "Multiple modes of electrical activities in a new neuron model under electromagnetic radiation," *Neurocomputing*, vol. 205, pp. 375–381, 2016.

[10] F. Q. Wu and H. G. Gu, "Bifurcations of negative responses to positive feedback current mediated by memristor in a neuron model with bursting patterns," *International Journal of Bifurcation and Chaos*, vol. 30, no. 04, p. 2030009, 2020.

[11] F. Q. Wu, H. G. Gu, and Y. Y. Li, "Inhibitory electromagnetic induction current induces enhancement instead of reduction of neural bursting activities," *Communications in Nonlinear Science and Numerical Simulation*, vol. 79, p. 104924, 2019.

[12] S. Qiao and X. L. An, "Dynamic response of the e-HR neuron model under electromagnetic induction," *Pramana*, vol. 95, no. 2, p. 72, 2021.

[13] S. Qiao and X. L. An, "Dynamic expression of a HR neuron model under an electric field," *International Journal of Modern Physics B*, vol. 35, no. 02, p. 2150024, 2021.

[14] H. R. Lin, C. H. Wang, and Y. M. Tan, "Hidden extreme multistability with hyperchaos and transient chaos in a Hopfield neural network affected by electromagnetic radiation," *Nonlinear Dynamics*, vol. 99, no. 3, pp. 2369–2386, 2020.

[15] H. Bao, D. Zhu, W. B. Liu, Q. Xu, M. Chen, and B. Bao, "Memristor synapse-based morris–lecar model: bifurcation analyses and FPGA-based validations for periodic and chaotic bursting/spiking firings," *International Journal of Bifurcation and Chaos*, vol. 30, no. 03, p. 2050045, 2020.

[16] K. X. Li, H. Bao, H. Z. Li, J. Ma, Z. Hua, and B. Bao, "Memristive Rulkov neuron model with magnetic induction effects," *IEEE Transactions on Industrial Informatics*, vol. 18, no. 3, pp. 1726–1736, 2022.

[17] F. Parastesh, K. Rajagopal, A. Karthikeyan, A. Alsaedi, T. Hayat, and V. T. Pham, "Complex dynamics of a neuron model with discontinuous magnetic induction and exposed to external radiation," *Cognitive Neurodynamics*, vol. 12, no. 6, pp. 607–614, 2018.

[18] S. J. Wang, S. B. He, K. Rajagopal, A. Karthikeyan, and K. Sun, "Route to hyperchaos and chimera states in a network of modified Hindmarsh-Rose neuron model with electromagnetic flux and external excitation," *The European Physical Journal - Special Topics*, vol. 229, no. 6-7, pp. 929–942, 2020.

[19] K. Rajagopal, I. Moroz, A. Karthikeyan, and P. Duraisamy, "Wave propagation in a network of extended Morris–Lecar neurons with electromagnetic induction and its local kinetics," *Nonlinear Dynamics*, vol. 100, no. 4, pp. 3625–3644, 2020.

[20] A. Karthikeyan, I. Moroz, K. Rajagopal, and P. Duraisamy, "Effect of temperature sensitive ion channels on the single and multilayer network behavior of an excitable media with electromagnetic induction," *Chaos, Solitons & Fractals*, vol. 150, p. 111144, 2021.

[21] S. L. Kingston, K. Suresh, K. Thamilmaran, and T. Kapitaniak, "Extreme and critical transition events in the memristor based Liénard system," *The European Physical Journal - Special Topics*, vol. 229, no. 6-7, pp. 1033–1044, 2020.

[22] S. Qiao, C. H. Gao, X. L. An, X. He, and J. Wang, "Electrical activities, excitability and multistability transitions of the hybrid neuronal model induced by electromagnetic induction and autapse," *Modern Physics Letters B*, vol. 36, no. 12, p. 2250006, 2022.

[23] C. H. Gao, S. Qiao, and X. L. An, "Global multistability and mechanisms of a memristive autapse-based Filippov Hindmash-Rose neuron model," *Chaos, Solitons & Fractals*, vol. 160, p. 112281, 2022.

[24] K. Rajagopal, S. Jafari, A. Karthikeyan, and A. Srinivasan, "Effect of magnetic induction on the synchronizability of coupled neuron network," *Chaos: An Interdisciplinary Journal of Nonlinear Science*, vol. 31, no. 8, p. 083115, 2021.

[25] K. Rajagopal, S. He, P. Duraisamy, and A. Karthikeyan, "Spiral waves in a hybrid discrete excitable media with electromagnetic flux coupling," *Chaos*, vol. 31, no. 11, p. 113132, 2021.

[26] X. L. An and L. Zhang, "Dynamics analysis and Hamilton energy control of a generalized Lorenz system with hidden attractor[J]," *Nonlinear Dynamics*, vol. 94, pp. 2995–3010, 2018.

[27] X. L. Song, W. Y. Jin, and J. Ma, "Energy dependence on the electric activities of a neuron," *Chinese Physics B*, vol. 24, no. 12, p. 128710, 2015.

[28] Y. M. Yang, J. Ma, Y. Xu, and Y. Jia, "Energy dependence on discharge mode of Izhikevich neuron driven by external stimulus under electromagnetic induction," *Cognitive Neurodynamics*, vol. 15, no. 2, pp. 265–277, 2021.

[29] S. L. Guo, J. Ma, and A. Alsaedi, "Suppression of chaos via control of energy flow," *Pramana - Journal of Physics*, vol. 90, no. 3, pp. 267–283, 2018.

[30] F. Q. Wu, T. Hayat, X. L. An, and J. Ma, "Can Hamilton energy feedback suppress the chameleon chaotic flow," *Nonlinear Dynamics*, vol. 94, no. 1, pp. 669–677, 2018.

[31] X. L. An and S. Qiao, "The hidden, period-adding, mixed-mode oscillations and control in a HR neuron under electromagnetic induction," *Chaos, Solitons & Fractals*, vol. 143, p. 110587, 2021.

[32] A. K. Tsaneva, H. M. Osinga, and T. Rie, "Full system bifurcation analysis of endocrine bursting models," *Journal of Theoretical Biology*, vol. 264, no. 4, pp. 1133–1146, 2010.

[33] J. L. Hindmarsh and R. M. Rose, "A model of neuronal bursting using three coupled first order differential equations," *Proceedings of the Royal Society of London, Series B: Biological Sciences*, vol. 221, no. 1222, pp. 87–102, 1984.

[34] K. J. Wu, T. Q. Luo, H. W. Lu, and Y. Wang, "Bifurcation study of neuron firing activity of the modified Hindmarsh–Rose model," *Neural Computing & Applications*, vol. 27, no. 3, pp. 739–747, 2016.

[35] A. Dhooge, W. Govaerts, and Y. A. Kuznetsov, "Matcont," *ACM Transactions on Mathematical Software*, vol. 29, no. 2, pp. 141–164, 2003.

[36] Y. Yang, X. Liao, and T. Dong, "Period-adding bifurcation and chaos in a hybrid Hindmarsh–Rose model," *Neural Networks*, vol. 105, pp. 26–35, 2018.

[37] R. Barrio, M. Lefranc, M. A. Martínez, and S. Serrano, "Symbolic dynamical unfolding of spike-adding bifurcations in chaotic neuron models," *EPL*, vol. 109, no. 2, p. 20002, 2015.

[38] Q. Xu, X. Tan, D. Zhu, H. Bao, Y. Hu, and B. Bao, "Bifurcations to bursting and spiking in the Chay neuron and their validation in a digital circuit," *Chaos, Solitons & Fractals*, vol. 141, p. 110353, 2020.

[39] X. B. Rao, X. P. Zhao, J. S. Gao, and J. G. Zhang, "Self-organizations with fast-slow time scale in a memristor-based Shinriki's circuit," *Communications in Nonlinear Science and Numerical Simulation*, vol. 94, no. 3, p. 105569, 2021.